ELSEVIER

Contents lists available at ScienceDirect

Additive Manufacturing

journal homepage: www.elsevier.com/locate/addma





3D printing of continuous fiber-reinforced thermoset composites

Xu He^a, Yuchen Ding^a, Zepeng Lei^b, Sam Welch^a, Wei Zhang^b, Martin Dunn^a, Kai Yu^{a,*}

- ^a Department of Mechanical Engineering, University of Colorado Denver, Denver, CO 80204, USA
- ^b Department of Chemistry, University of Colorado Boulder, Boulder, CO 80309, USA

ARTICLE INFO

Keywords:
3D printing
Direct ink writing
Continuous fiber
Thermoset composites

ABSTRACT

Current printing methods for continuous fiber-reinforced composites require the composites to quickly solidify during the printing, so the matrix is limited to thermoplastics or thermosets with fast curing mechanisms. This paper presents the first design of a 3D printer head for direct-ink-writing that can overcome the limitations on printable resins. It leverages the shear stress imposed on the fiber to enable the ready extrusion of composite filaments and is applicable to a wide variety of thermoset resins and commercially-available continuous fibers. The developed printing method can create thermally-curable composite components with covalently bonded interfaces and comparable mechanical strength as directly-molded samples. It also enables the free-standing 3D printing of UV-curable composites. Overall, the developed printing method allows the composite parts to be designed quickly to meet unique specifications, as well as provides new functions in 4D printing, biomedical printing, and the printing of functional devices.

1. Introduction

Continuous fiber-reinforced thermoset composites, with their superior combination of stiffness, strength, and lightweight, have been leading contenders in various applications ranging from aerospace to ground transportation [1,2]. Conventional manufacturing methods, such as the injection molding, filament winding, and pultrusion, use expensive molding tools to shape the resin and fibers [3]. Mass production is required to even out the overhead cost of tooling, labor for assembly, and production. The economic barrier to create complex structures or change the design of composite products is significant. In great contrast, 3D printing enables the moldless fabrication of composite parts with no additional cost for geometric complexity. The high design freedom and low cost-per-part make it ideal for rapid prototyping and product development [4–8]. In addition, it allows the user to easily design composites with tailored fiber distribution and selective reinforcements [9–11].

Among a variety of polymer 3D printing techniques, the extrusion-based printing methods [5,12,13] show the great promise in fabricating continuous-fiber reinforced composites. For example, Matsuzaki et al. [14] customized the fused deposition modeling (FDM) printer to fabricate composites using in-nozzle impregnation. The polylactic acid (PLA) filament and continuous fibers were separately supplied to the printer head. Various composite filaments and printers (e.g.,

Markforged, Watertown, MA) have been commercialized to print composites with a pre-determined resin-fiber combination. However, the FDM-based methods are limited to the printing of thermoplastics composites, which do not typically possess the stiffness and strength for high-performance applications.

The direct ink writing (DIW) technique allows for the printing of a wide range of thermosetting polymers [9,11,15-20]. The extruded filaments can be polymerized by applying UV light during the printing (for UV-curable resin) [18,21] or transferring the filaments into a heating oven for curing (for thermally-curable resin) [9,11,15,20]. Different DIW printer heads have been conceptually designed by researchers to print continuous fiber-reinforced thermoset composites [22,23]. However, to the best of our knowledge, there is no detailed report on how to realize and practice these designs. For example, the patent [23] proposes a DIW printing method for carbon fiber reinforced epoxy. The fiber is fed into the syringe to meet the resin through a hollow tube. The backflow of resin at the end of the feeding tube would prevent the fiber extrusion. Continuous Composite Inc. (Coeur d'Alene, ID) patented the design of a DIW printer head for UV-curable thermoset composites with continuous fiber [24]. The printer head comprises a syringe for resin storage, a deposition nozzle, a feeder for continuous fiber, and a UV lamp for photo-polymerization. The fiber feeder connects to the syringe through a one-way check valve, which prevents the backflow of liquid resin into the feeder. However, the check valve also applies considerable friction

E-mail address: kai.2.yu@ucdenver.edu (K. Yu).

 $^{^{\}ast}$ Corresponding author.

for fiber extrusion. Therefore, the deposited composite filaments are required to quickly solidify and stick to the stage during the printing, which provides a persistence force to hold the filament in place and pull the fiber when the printer head moves forward.

Due to the early stage of development, limitations exist in the current designs of printer heads for the continuous-fiber composites. First, the printable material is limited to the thermoplastics or thermosets with fast curing mechanism, such as the UV-curable resins or the recently developed resin with exothermic frontal polymerization [25,26]. There has been no robust design of printer head to print thermally-curable continuous fiber composites, which are widely used as in the composite industry. For example, it was reported that the thermally-curable epoxy, polyester, vinyl ester, and polyurethane share over 91% of the global thermoset resin market in the composite industry [27]. Second, printed composites usually suffer from low quality and mechanical properties. When using thermoplastics or UV-curable resin as composite matrixes, the filament interfaces are bonded primarily by the non-covalent bonds and thus exhibit weak interfacial strength [28–31]. Third, due to the presence of gaps between solidified filaments, 3D printed composites usually show significant void formation (\sim 20%) [7, 32–34], which generates stress concentration during the deformation and compromises the mechanical properties of the printed composites [32,35,36].

In this work, we developed a versatile 3D printing method for the continuous fiber-reinforced thermoset composites, which removes the limitations of the printable resins. It leverages the shear stress imposed on the fiber by the viscous ink to enable the ready extrusion of composite filaments and is applicable to a wide variety of thermally-curable and UV-curable composites. To demonstrate the versatility of the developed printing method, a thermally-curable polyimine and UV-curable acrylate are respectively adopted as the composite matrix. After printing polyimine composites, the components are transferred into an oven for post-curing. The interfacial polymerization leads to strong interfaces connected by the covalent bonds. During the post-curing, the slight viscous flow of thermoset resin helps close the micro-voids between filaments and thus improves the mechanical performance of printed composites. In this manner, the printed composite laminates exhibit comparable stiffness and strength as directly molded samples. The developed printing method was also applied to printing photo-curable composites with UV sources attached to the sides of the printer head. During the printing, the matrix resin quickly solidifies and holds the composite filaments in place. Since there is negligible force applied on the filaments after their extrusion, the developed printing method enables the free-standing 3D printing without sacrificial materials and the deposition of the composite layer on curved surfaces. Overall, this study provides a robust platform for printing thermoset composites with essentially no restriction on the printable materials and fibers, which greatly facilitates the digital design and rapid prototyping of modern composite products. It also dramatically expands the scope of printable materials for the emerging technologies in 4D printing, biomedical printing, and the printing of functional devices.

2. Material and methods

2.1. Design of the printer head

The customized DIW printer setup is illustrated in Fig. 1. The printing head comprises of a deposition syringe connected to a digital pneumatic regulator (Ultimus V high precision dispenser, Nordson EFD). The regulator can provide a deposition pressure ranges from 0 to 100 psi. The deposition syringe is mounted onto a moving stage (Makerbot, New York, NY), and its motion is controlled by the computer. The digital dispenser provides a controlled pressure, which is split into two streams, P_1 and P_2 , and applied to the deposition syringe.

The detailed design of the printer head is illustrated in Fig. 2. The thermoset resin with a suitable viscosity is loaded in the syringe as the printable ink. The commercial carbon fiber bundle (with 6k T300 carbon fibers, diameter ~ 9 um) without chemical treatment is fed into the syringe through a feeding tube. Note that other types of high-strength fibers (e.g., glass fiber) can also be adopted as composite reinforcement. Two pressures are supplied to the deposition syringe (P_1 and P_2). When

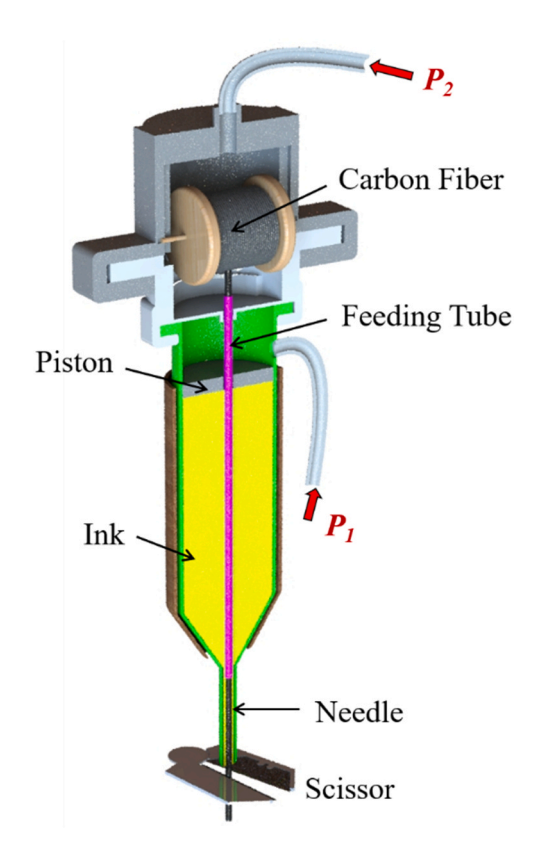


Fig. 2. Cross sectional view of the designed DIW deposition syringe.

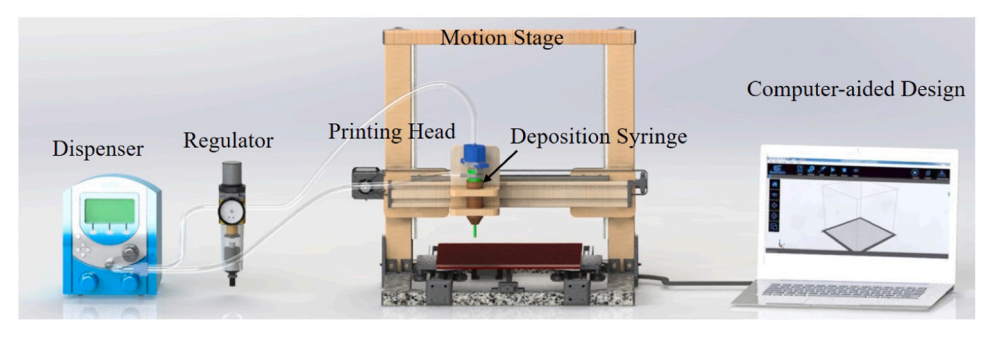


Fig. 1. Schematic view of the designed DIW printer for the continuous fiber-reinforced thermoset composites.

the deposition pressure P_1 is applied, it pushes the piston for ink deposition. The ink viscous flow within the needle section applies shear stress on the fiber, which drives its flow through the nozzle. To prevent the backflow of the ink into the feeding tube, a positive pressure P_2 is applied on the top to balance the pressure at the end of the tube. Compared to the existing designs of printer head, the presented one does not require the filament to be quickly solidify because i) the driving force for filament extrusion is provided by the shear stress applied on the fiber by viscous resin, and ii) the design uses a pressure to prevent the ink backflow, which does not apply notable frictions to resist the fiber extrusion. It is important to note that the designed printer head is independent of the dynamics of the motion stage, and thus can be readily connected to other printing platforms.

2.2. Preparation of the thermally- and UV-curable printable inks

The developed printing method for thermoset composites has a great potential in printing a wide variety of thermally- and UV-curable resins. For thermally-curable resin, the printable inks can be prepared by partially curing the monomers and cross-linkers at high temperatures until the suitable rheological properties are reached. Nano-clay can be added into the mixture to introduce the shear thinning-effect and enhance the ink shear strength. In this paper, a polyimine thermoset is adopted. The printable ink can be prepared by mixing the monomer terephthaldehyde (dialdehyde), monomer diethylenetriamine (diamine), and cross-linker tris (2-aminoethyl) amine. All these chemicals are purchased from the Sigma Aldrich (St. Louis, MO, USA), and their detailed chemical structures are shown in the Supplementary Materials (Section S1). According to Taynton et al. [37], the mole ratio among these chemicals is 1: 0.3: 0.467 and the curing temperature is between 75 °C and 105 °C.

An alternative approach to prepare the thermally-curable polyimine inks is to utilize the solvent-assisted recycling mechanism [38-42]. The polyimine networks contain imine bonds in the backbone. When the polymer is soaked in the amine-containing solvents, the amine molecules diffuse into the network, break the imine bonds through bond exchange reactions [43-49], and eventually depolymerize the network. Since the reactions are reversible, re-polymerization can occur via heating the decomposed polymer solution in an open environment. Based on this recycling mechanism, a fully-cured polyimine thermoset was first decomposed in propylamine solvent at 50 °C for 30 mins, which produced a mixture of starting monomer, crosslinker, and excessive solvent. Nanoclay was then added, and the mixture was heated at 80 °C with a vacuum level of 8 kPa. After evaporating the excessive solvent, the re-polymerization was triggered, which increased the mixture viscosity. Both two approaches are equally effective for producing thermally-curable printable inks with suitable viscosity. In this work, the second approach was adopted when examining the repeatability of the developed printing method.

The printable acrylate ink for UV-curable thermosets and their composites was prepared by mixing monomer 2-hydroxy-3-phenoxy-propyl acrylate and crosslinker bisphenol A glycerolate diacrylate. Their mole ratio was 1:2. The detailed chemical structures are shown in the Supplementary Material. 2 wt% of diphenyl (2,4,6-trimethylbenzoly) phosphine oxide (compared to the total weight of solution) was added into the mixture as the photo initiator. All the chemicals were purchased from the Sigma Aldrich.

2.3. Ink rheological measurements

To print the thermally-curable polyimine composites, the ink rheological properties are important to control so the printouts can maintain their filament geometry after extrusion. The rheological properties of the prepared polyimine ink were measured using a rheometer (TA Instruments, AR-G2, New Castle, DE, USA). It was equipped with parallel plates with a diameter of 20 mm and a plate gap of 1 mm. To determine

the rate-dependent viscosity, viscometry measurements were first carried out at room temperature, and the shear rate ranged from 10^{-3} to $200~{\rm s}^{-1}$. To determine the shear modulus of the polyimine ink, oscillatory measurements were performed at a frequency of 1 Hz within the stress range of $0.01-10,000~{\rm Pa}$. The measured shear modulus was used to identify the shear yielding stress, which was taken to be the stress when the modulus started to drop abruptly.

2.4. Post curing

Right after printing the polyimine composites, the matrix contained unreacted solvents and remained in the gel state. A post-curing step is therefore needed to fully polymerize the material. The post-curing was performed in a vacuum oven with 8 kPa vacuum pressure applied. To avoid the melting of the polyimine matrix, the initial heating temperature was set to be 45 $^{\circ}$ C. After being heated for 2 h, the polyimine matrix gained sufficient modulus and could maintain the composite structure. Subsequently, the temperature was further increased to 80 $^{\circ}$ C. After being heated for another 6 h, the printed polyimine composites were fully polymerized.

2.5. Uniaxial tension

To examine the mechanical properties (e.g., elastic modulus and strength) of the printed thermosets and their composites, uniaxial tension tests were performed on a Bose electro-force test instruments (3200 series II, New Eden Prairie, MN, USA). The specimen dimension for uniaxial tension tests is 20 mm in width and 45 mm in length. The specimen has three printed layers, and its thickness is roughly three times of the filament diameter. All the tension tests were performed at the room temperature ($\sim\!23~^\circ\mathrm{C}$) with a strain loading rate of 2%/s. After tests, the initial elastic modulus was calculated from the initial loading stage at 2% engineering strain, and the ultimate strength was also reported.

3. Results and discussion

3.1. Selection of deposition pressure for filament extrusion

To enable the steady extrusion of composite filaments, the ink rheological properties and deposition pressures (P1 and P2) are important parameters to control. For the filament-based DIW process, the printable ink is required to readily flow through fine nozzles assisted by its shear-thinning effect and retains the filamentary form upon deposition due to a high modulus and yielding stress. Typical values of the ink apparent viscosity and shear yielding stress are 10^{-1} 10^{3} mPa s (depending on the shear rate) and 10-100 Pa, respectively. To prepare the printable polyimine ink, the precursor monomers were partially cured by heating at 80 °C. The solution viscosity increased as the polymerization proceeded. 10 wt% nano-clay (compared to the total solution weight) was added to introduce the shear-thinning effect and improve the capability of filaments to support themselves after deposition. The ink rheological properties were tested using the rheometer (TA Instruments, AR-G2, New Castle, DE, USA). As shown in Fig. S2, after being heated for 20 mins, the ink possessed a viscosity of \sim 4.4 \times 10³ Pa's at low shear rates $(1 \times 10^{-3} \text{ s}^{-1})$. Due to its strong shear thinning behavior, the ink exhibited an apparent viscosity of ~110 Pa's at shear rates (~50 s⁻¹) typically experienced during printing. The shear storage modulus at the low-stress level and the shear yielding stress were ${\sim}10\text{kPa}$ and ${\sim}200$ Pa, respectively. Using the same pre-curing method, other commercial thermoset resins (e.g., epoxy, polyester) can also be adopted to print continuous-fiber composites using the designed printer

Among the two pressures, P_1 controls the extrusion velocity and P_2 determines the smooth deposition of the composite filament. As shown in Fig. 3, when P_2 is lower than the pressure at the junction between the

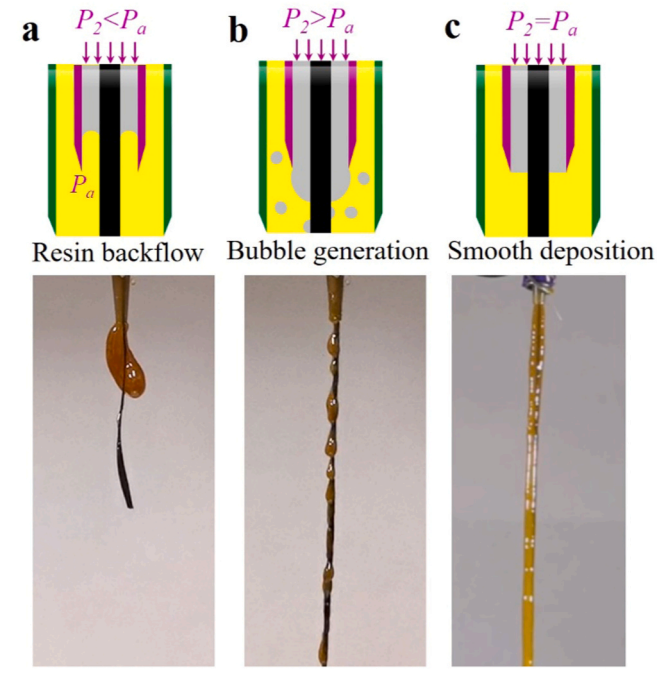


Fig. 3. Filament extrusion with different P_2 values. Smooth filament extrusion can be realized when the secondary pressure, P_2 , equals to the junction pressure within the syringe, P_a .

converging section and the needle section of the syringe (P_a) , only the ink can be extruded while the fiber bundle is stable. A lower P_2 leads to the notable backflow of printable inks from the deposition syringe into the feeding tube, which resists the fiber movement. On the other hand, when P_2 is higher than the junction pressure, the fiber bundle is seen to be extruded quickly, but bubbles are generated within the ink, which leads to the discontinuous cladding of the resin around the fiber. A smooth deposition (as shown in the Supplementary Video 1) can be realized by setting P_2 equal to the junction pressure.

Supplementary material related to this article can be found online at doi:10.1016/j.addma.2021.101921.

Since it is challenging to monitor the pressure distribution within the syringe during the filament extrusion, a fluid-mechanics model is established in Section S4 of the Supplementary Material to calculate the junction pressure Pa, and thus determine the magnitude of the secondary pressure (P2) to be applied. Within the model, the syringe is split into three sections with a uniform inlet section followed by a converging section leading to another uniform needle section for filament extrusion. The model considers the flow rate of a fully developed non-Newtonian low-Reynold viscous liquid within the syringe and can predict the junction pressure based on the ink apparent viscosity and deposition pressure P₁. The calculated secondary pressure (P₂), which equals to the junction pressure Pa, is plotted in Fig. S4b as a function of input deposition pressure (P₁). The model serves as an effective computational tool to guide the printing process of composite samples and structures in the following sections. It also allows our future study to examine the influences of syringe geometry and other process parameters on the printing process.

3.2. Filament extrusion speed and morphology

After extrusion, the continuous filaments were cut using a scissor and transferred to an oven for post-curing. Initially, a relatively low temperature (45 $^{\circ}\text{C}$) was used to polymerize the matrix gradually and lock the printed shape with a sufficiently high modulus. After 2 h, the curing temperature was increased to 80 $^{\circ}\text{C}$. The polyimine matrix was fully polymerized after $\sim\!6$ h.

The cross-sectional views of fully-cured composite filaments were acquired using a microscope (Keyence VHX-7000, Itasca, IL). Since the deposition of composite filaments is driven by the shear stress applied on the fiber bundle, they can be printed with a circular cross-section, with the fiber bundle located in the filament center (Fig. 4a). The fiber content can be calculated based on the cross-sectional areas of the composite filament and carbon fibers. It can be tailored by changing the size of dispenser needle. Four types of needle with inner diameters of 2.41 mm, 1.83 mm, 1.27 mm, and 0.91 mm were used, and the corresponding fiber volume fractions were 8%, 15%, 30%, and 59%, respectively, when the deposition pressure was 40 psi. The newly designed printer head was able to print filaments with fiber content up to 36%. Fig. 4b shows the morphology of the fiber in the filament crosssection. It is observed that the resin fully permeates inside the fiber bundle. The good impregnation of fiber will enable the fabrication of high-quality composites without voids and promote the bonding strength between fiber bundle and matrix, leading to their efficient load transfer.

The filament extrusion velocity was tested with different deposition pressures, P₁, and needle diameters (Fig. 4c). During the testing, the filament extrusion process was recorded by a video camera to measure the velocity. The pressure, P₂, was calculated using the fluid-mechanics model presented in the Supplementary Material. It was observed that the extrusion velocity increased with both pressure and needle size. For each needle diameter, the velocity can be tailored from around one millimeter per second up to a few centimeters per second, and such control was shown to be stable and repeatable. Fig. 4d shows the diameter of extruded filaments with different deposition pressures and needle diameters. After the printable ink existing the needle, it tended to swell since the hydrostatic pressure dropped to zero, which is commonly known as the die swelling effect. Because of this, the diameter of composite filaments increased as getting out of the needle tip. The increment was higher when a smaller diameter or higher deposition pressure was used. For example, the filament diameter was measured to be 1.29 mm when the needle diameter was 0.91 mm and the deposition pressure was 80 psi. This is corresponding to a ~42% diameter increment, while the increment is only ~12% when the needle diameter is 2.41 mm.

The filament extrusion is driven by the shear force applied by the ink on the fiber bundle. In the Supplementary Material (Section S5), the shear force on the fiber bundle is calculated based on the measured extrusion velocity of filaments. As shown in Fig. S6, the shear force increases with the deposition pressure and extrusion velocity. A smaller needle diameter typically leads to a higher shear force. For the 0.91 mm needle diameter, the highest shear force is ~ 0.034 N. During the filament extrusion, there exists friction between the fiber bundle and feeding tube, as well as the rotational friction from the fiber bubbin. To optimize the design of the deposition syringe, the frictions on the fiber bundle should be minimized, and the driving shear force on the fiber bundle should overcome these frictions to ensure a steady-state filament extrusion.

3.3. Mechanical properties of the printed thermally - curable composites

To evaluate the mechanical properties of the printed thermoset composites, a laminate sample was printed with three layers, and the fiber bundles were aligned in the same direction in each layer. During the printing, the deposition pressure was 40 psi, and the needle diameter was 1.83 mm. To enable the smooth filament deposition, the traveling speed of the deposition head was set to be the same as the filament extrusion speed (as shown in Supplementary Video 2). The fiber volume content of the composite filaments was \sim 9%. The deposition spacing between the filaments was set to be 1.1 mm, which was \sim 87% of the filament diameter. After printing, the sample was transferred to a heating oven for post-curing. The printed laminate and the cross-sectional view are respectively shown in Fig. 5a and b. There was no defect on the surface of the printed samples after post-curing. The fiber

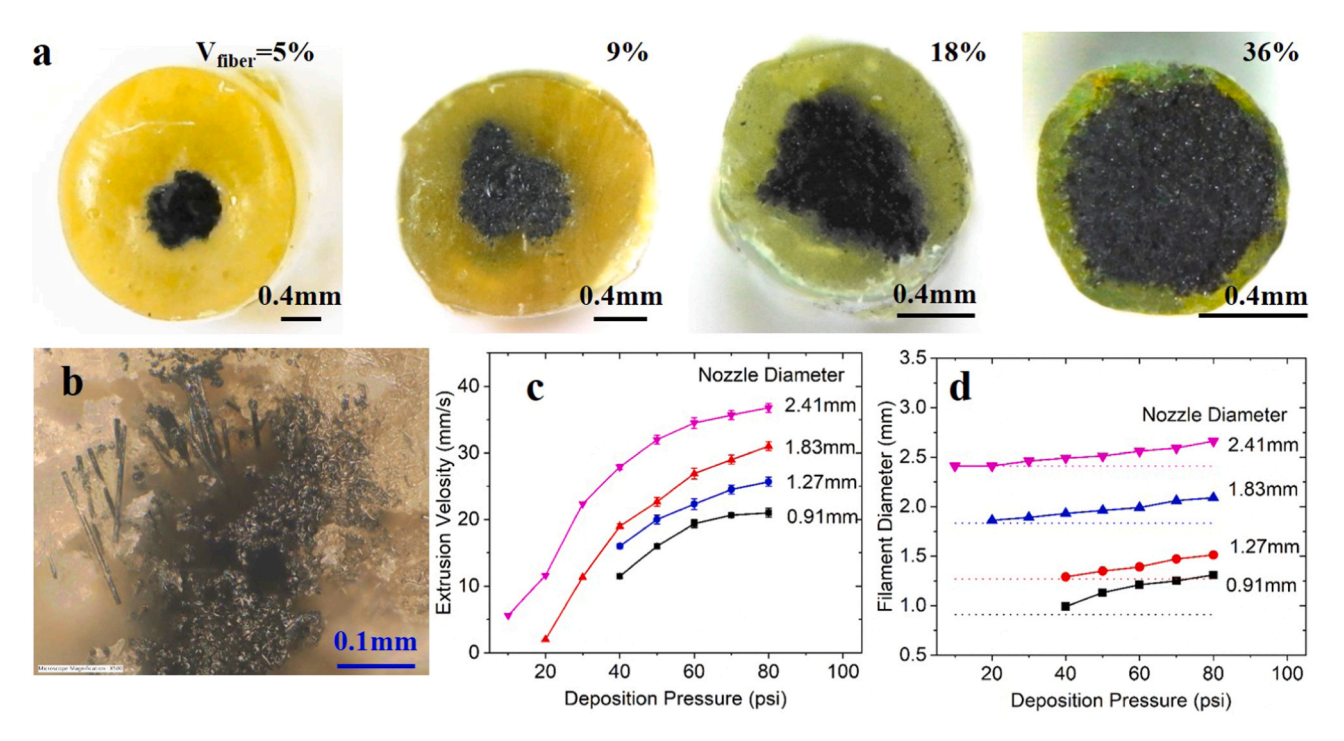


Fig. 4. Filament morphology, extrusion speed, and fiber content. (a) Cross-section views of composite filaments with different fiber contents. (b) microscopic morphology of the fiber bundle on the filament cross-section. (c) Extrusion speed with different deposition pressures and needle diameter. (d) Filament diameter with different deposition pressures and needle diameter.

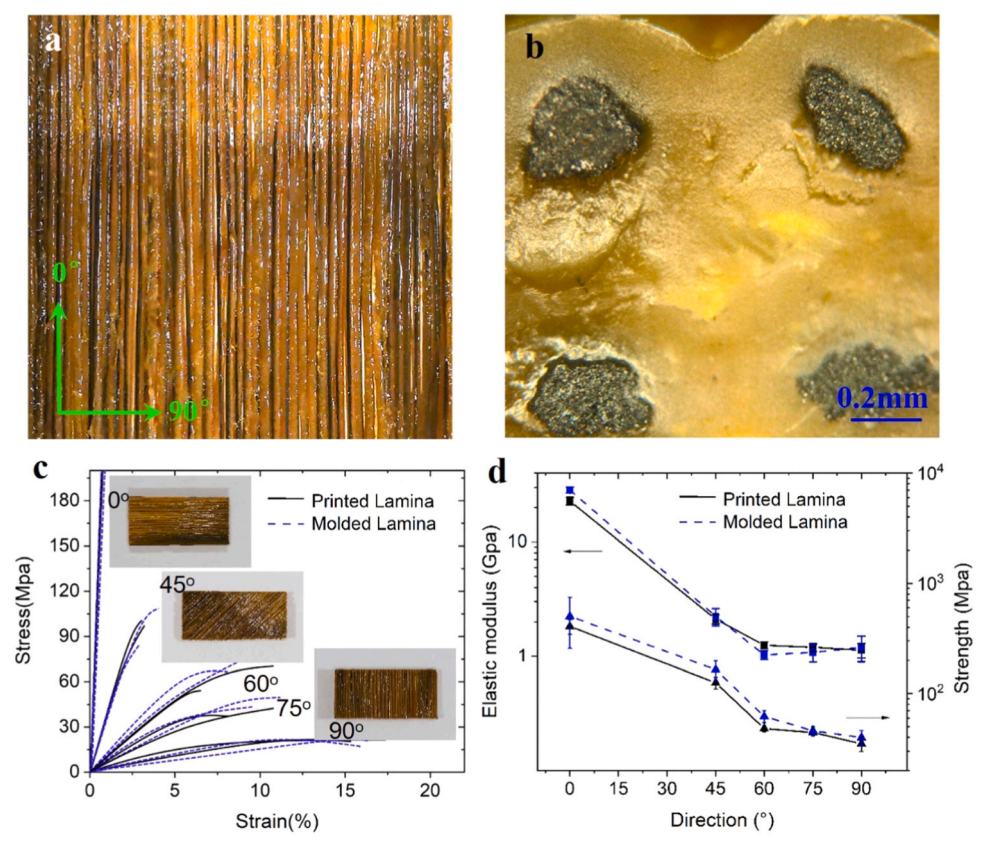


Fig. 5. Mechanical properties of printed thermally-curable composites. (a) Tensile specimen is cut in different directions with respect to the fiber. (b) Cross-sectional view of the printed composite laminate. (c) Room-temperature stress-strain curves. (d) Elastic modulus and ultimate strength compared to the directly molded sample.

bundles were observed to align well with each other, indicating a good deposition precision. As a control sample, a composite laminate was fabricated using the direct molding process with the same fiber content and orientation.

Supplementary material related to this article can be found online at doi:10.1016/j.addma.2021.101921.

Tensile specimens were cut in different directions $(0^{\circ}, 45^{\circ}, 60^{\circ}, 75^{\circ},$ and 90°) with respect to the fiber orientation. The specimens were manually cut using a razor into identical dimension (width = 20 mm and thickness = 45 mm), the sample thickness is roughly three times of the filament diameter, which depends on the fiber content. After cutting, the specimens were carefully polished using a sandpaper to maintain a rectangular geometry. The inset pictures of Fig. 5c show the appearances of the prepared specimen. The specimen was then subject to the uniaxial tension tests on Bose electro-force test instruments (3200 series II. New Eden Prairie, MN, USA). The glass transition behavior of the polvimine matrix was tested, and the results are shown in Fig. S3 (Supplementary Material, Section S3). The glass transition temperature (T_{σ}) of the polyimine matrix is around 55 °C, which indicates that the composites are in the glass state at room temperature without viscoelastic effects. All the tension tests were performed at room temperature, and the strain rate were 2%/min in all cases.

Fig. 5c shows the stress-strain relations of the printed and directly-

molded laminate in different directions of carbon fiber. Their elastic moduli (within the first 2% of strain) and ultimate strength are summarized in Fig. 5d. It is prominent to observe that the printed laminates exhibit comparable mechanical properties as the directly-molded samples in all directions, especially when the loading direction is vertical the fiber, and the filament interfaces are being stretched. This is mainly attributed to two mechanisms during the post-curing of printed composites. First, the interfacial polymerization among filaments leads to strong interfaces connected by covalent bonds, which are primarily the C⁻N bonds on the chain backbone. The interfacial covalent bonding prevents the laminate breaking through filament delamination. Second, due to the slight viscous flow of thermoset resin during the post-curing, the composite filaments can be fully fused together with their interfaces disappeared. No defect or noticeable void was observed within the structure (Fig. 5b). It is important to note that the microscopic viscous flow of thermoset resin did not result in a noticeable macroscopic shape change of the composite dimension. The excellent mechanical performance of the printed composites represents a sustainable improvement compared to the previously printed thermoplastics and photo-curable thermoset composites, in which the filament interfaces were connected mainly by the weak non-covalent bonds [31] (e.g., van der Waals force), and noticeable void formation was observed within the composite structures [32,35,36].

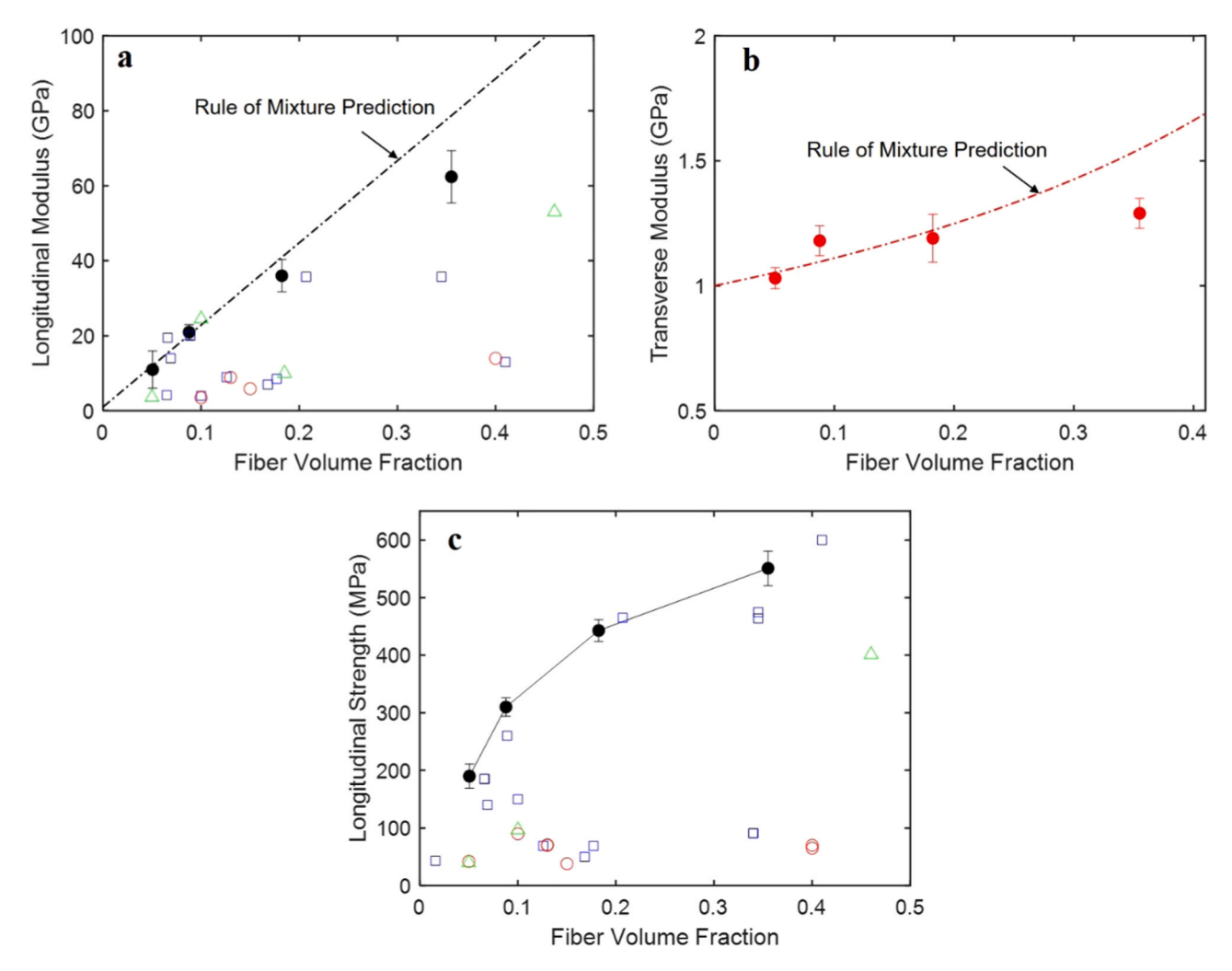


Fig. 6. Mechanical properties of printed composites with different fiber contents: (a) The longitudinal modulus, (b) the transverse modulus, and (c) ultimate strength of the printed composites. The data points in (a) and (c) are collected in existing studies on composite 3D printing, including the continuous carbon fiber thermoplastic composites printed with FDM [14,50–57] (blue squared dots), short carbon fiber thermoplastic composites printed with FDM [58–61] (red circular dots), and short carbon fiber thermoset composites printed with DIW [63–65] (green triangular dots). (For interpretation of the references to colour in this figure legend, the reader is referred to the web version of this article.)

The mechanical performance of printed composites with different fiber contents is examined. In the Supplementary Material (Section S6), Fig. S7a shows the elastic modulus and ultimate strength of printed composites with 36% carbon fiber. They are measured in different directions with respect to the fiber orientation. It is seen that the printed composites also exhibit comparable mechanical properties as the directly-molded samples in all directions.

The longitudinal modulus (along the fiber direction) and transverse modulus (vertical to the fiber) of the printed composites are summarized in Fig. 6a and b. The experimental data are plotted as solid circular dots. The modulus is shown to be substantially enhanced with the increment of fiber content. Specifically, the modulus is predicted by the Rule of Mixture, where the fiber modulus is taken to be 220 GPa. According to the DMA results in Fig. S3 (Supplementary Material, Section S3), the matrix modulus at room temperature is 0.96 GPa. The comparison in Fig. 6a and b shows the experimental results agree with the predictions well, despite that the modulus of printed composites with 36% fiber is slightly lower than the theoretical predictions.

The longitudinal modulus in Fig. 6a is also compared with results in existing studies on composites 3D printing, which include the continuous carbon fiber-reinforced thermoplastic composites printed with fused deposition modeling (FDM) [14,50–57] (blue squared dots), short carbon fiber-reinforced thermoplastic composites printed with FDM [58–61] (red circular dots), and short carbon fiber-reinforced thermoset composites printed with direct ink writing (DIW) [62–64] (green

triangular dots). Fig. 6c shows the longitudinal strength of the printed composites and comparison to existing studies. The printed composites in this work use the tough thermoset matrix and continuous carbon fiber as the reinforcement. There is no notable void among the filaments, and they are connected by substantial covalent bonding. Therefore, the printed composites exhibit higher modulus and ultimate strength at an equivalent fiber content compared to existing studies.

The highest fiber content in Fig. 6 is 36%. In the Supplementary Material (Section S6), a composite lamina with \sim 43% fiber is printed by using a smaller nozzle with a 0.83 mm diameter. While we can enable the steady extrusion of the filament, the printed composites exhibit weak mechanical performance compared to the directly molded sample with the same fiber content, especially the transverse strength. The reason might be that there is not enough resin on the surface of the filaments to enable their tight and covalent bonding. How to further increase the fiber content while maintaining the mechanical performance of the printed composites deserve our future study.

3.4. 3D printing of thermally-curable composite structures

Several composite architectures with varied geometries were printed, as shown in Fig. 7a (see the Supplementary Video 3 for the printing of the first architecture). Each structure has a unique fiber content by changing the nozzle diameter. The deposition pressure was set to be 40 psi for all cases. After printing, all the structures were subjected to the

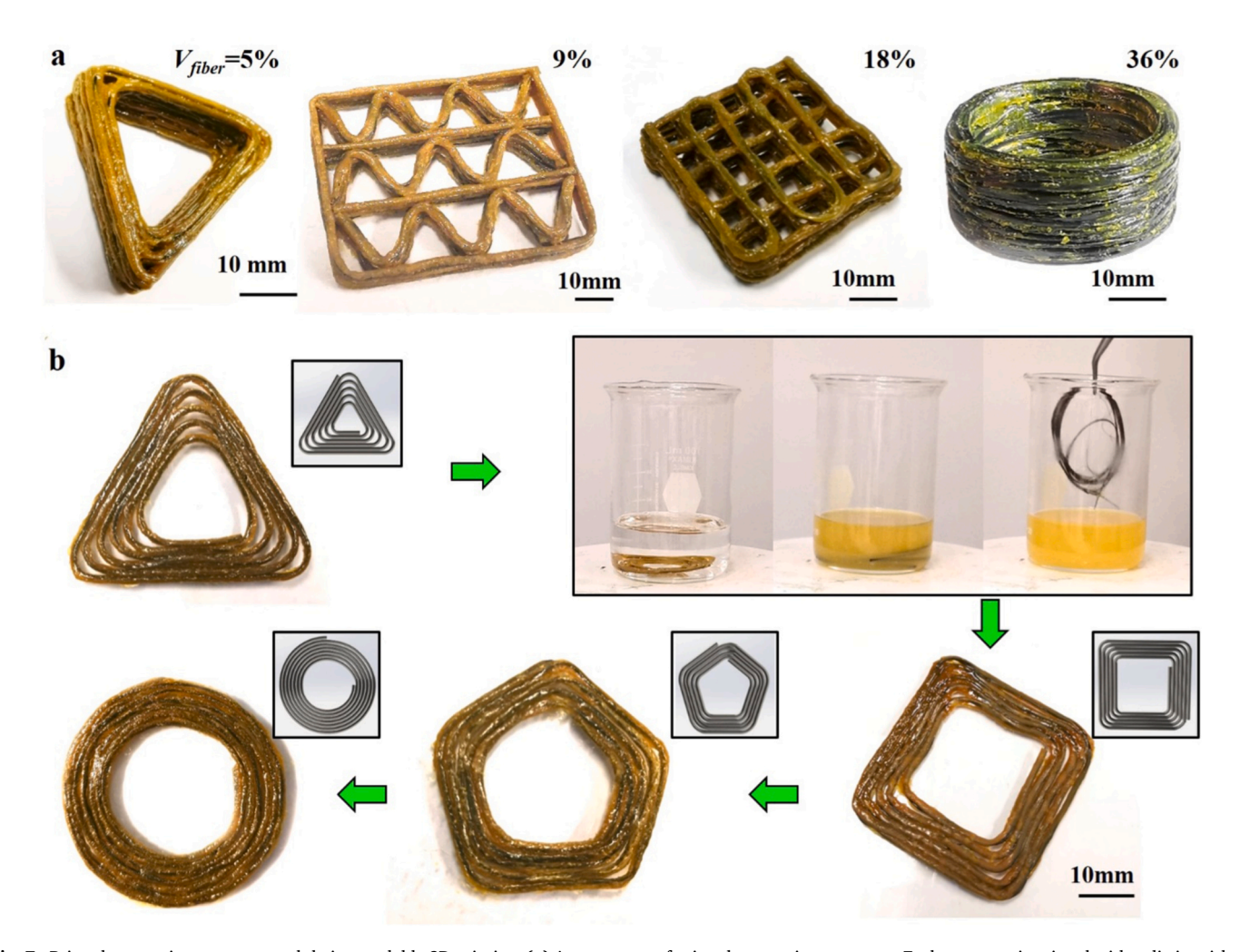


Fig. 7. Printed composite structures and their recyclable 3D printing. **(a)** Appearances of printed composite structures. Each structure is printed with a distinguished nozzle diameter and fiber volume content. **(b)** The recyclable 3D printing of fiber composites using organic solvent. The printed components are immersed in 80 °C solvent for 10 min. The polyimine matrix is fully decomposed and clean fibers are reclaimed. The decomposed polymer solution and fiber are loaded to the printer for the next round of 3D printing. This procedure is repeated for three times. Scale bars in all these figures are 10 mm.

post-curing under the same temperature conditions. The structure geometry and dimension were perfectly maintained after post-curing without collapse or notable shape distortion.

Supplementary material related to this article can be found online at doi:10.1016/j.addma.2021.101921.

Using smaller nozzles would further promote the printing resolution of the composite structures. Another unique consideration for the DIW printing of continuous-fiber composites is the intrinsic stiffness of the fiber bundle. Thin filaments with higher fiber content tend to bounce off from the printing pathway at the turning location, which would notably affect the printing resolution, especially at the joints of complex structures. Therefore, the DIW printing of continuous fiber-reinforced thermoset composites requires careful path planning to consider the influences of fiber stiffness. To examine the maximum printing curvature with different fiber content, composite filaments with 180° turning feature were printed (Fig. S8, Supplementary Material). It is seen that the thick filaments maintain the printing curvature as more resin holds the fiber in position. The maximum printing curvatures for the three higher fiber contents (9%, 18%, and 36%) are estimated to be 0.12, 0.48, and 1.7 mm⁻¹, respectively. When the composite components in Fig. 7a were printed with different fiber contents, we designed the printing path with the highest curvatures below the corresponding critical values. Therefore, the printed pattern can exactly match with the CAD model without notable shape distortions. The detailed relationship between maximum printable curvature, ink rheological properties, and fiber content will be under our further study and incorporated into the existing path planning algorism. For example, when the planned printing curvature is above the maximum value, an automatic scissor below the deposition needle should be triggered to cut the composite filaments.

To examine the repeatability of the developed printing method, we printed multiple composite components using the same batch bath of ink, the same fiber bundle, and identical deposition pressures. Conventional thermosets exhibit permanent crosslinking networks and thus cannot be recycled. But in this work, the adopted polyimine network contains imine bonds on the chain backbone [37,65], and was shown to be effectively depolymerized into precursor monomers in amine-containing solutions [40,65]. Since the imine linkage formation is reversible, re-polymerization can occur via heating the polymer solution in an open environment to remove the small molecule byproduct. Detailed recycling mechanism and operation process are described in the experimental section.

The recycling mechanism was utilized during the repeat printing of composite components. As shown in Fig. 7b, a triangular composite component with 9% fiber content was first printed with $P_1 = 40$ psi and $P_2 = 11$ psi. After the composite is fully cured, it was immersed in the propylamine solvent at 80 °C to decompose the matrix and reclaim the fiber bundle. Note that the primary recycling of the thermoset matrix is due to the reversible bond exchange reactions between network and solvent molecule, as reported in our previous work [37,40]. The decomposed polymer solution was partially cured at 80 °C for 10 mins and reloaded into the printer head with the reclaimed fiber bundle for the next round of printing. Such process was repeated for three times to print composite components in different geometries. Note that under the same processing conditions in each cycle, the ink exhibited identical rheological properties. During the printing, identical deposition pressure (P1 and P2) and needle diameter were used. The composite components were precisely printed without cracking or shape distortion. No printing adjustment or Supplementary Material was added during the printing process. Therefore, our newly designed printing method shows great repeatability and reliability in the printing of thermoset composites.

3.5. 3D printing of UV-curable thermosets and composites

To demonstrate its versatility, the developed printing method was further applied to print UV-curable thermosets and their composites. An acrylate-based thermoset was adopted with detailed formulation described in the experimental section. During the printing, two UV lamp chips (Shenzhen YM Technology Co., Ltd, China) were attached on each side with a ~15 cm distance to the needle tip. Each chip has 100 LED beads, and the power output is 20 W. With the applied UV intensity, the matrix can be quickly cured within seconds. As shown in the Supplementary Material (Section S8), the room temperature modulus of the matrix was increased to 500 MPa within 1 s, which helped the filament hold the position in place. To further enhance the shape fixing ability of the filament, a portable dental UV curing lamp (Foshan Horyn Medical Instrument Co., Ltd. China) with 2 W power output was applied close to the filament during the printing.

Uniaxial tension tests were performed on the printed UV-curable composites with 9% carbon fiber, and the results are shown in the Supplementary Material (Section S8). As shown in Fig. S11, the acrylate composites exhibit comparable modulus and longitudinal strength compared to the printed thermally-curable polyimine composites with the same fiber content. However, because the filaments are mainly connected via non-covalent bonding, the transverse strength (~19 MPa) is notably lower than that of the polyimine composites (~33 MPa).

Since the filament can be quickly solidified, and there was no external force applied on the filament after extrusion, free-standing 3D printing of thermoset components can be realized. As shown in Fig. 8a and b, an acrylate spring without and with carbon fiber bundle (volume fraction = 5%) can be both printed without Supporting Materials (Supplementary Video 4). Fig. 5c demonstrates that a lattice structure with 9% carbon fiber can be created, wherein each rod is printed at the designed positions and then manually cut after being welded at the joint.

Supplementary material related to this article can be found online at doi:10.1016/j.addma.2021.101921.

Modern composite products demand laying fiber on the 3D surface, which would enhance mechanical properties of objects, or introduce electrical and thermal functions. By properly designing the printing pathway, the developed printing method was able to deposit the fiber composites on the curved surfaces, including a wavy and spherical surface (Supplementary Video 5). Specifically, the coating on the spherical surface was realized by depositing a single composite filament along a spiral pathway. The fibers are evenly distributed. Overall, 3D printing of UV-curable composites using the developed printing method enables the placement of reinforcement fibers in the 3D space with or without substrate support, thus overcoming the manufacturing limitations in the conventional approaches. It shows great potential to open new avenues for composite design and dramatically expedite the development of new composite products.

Supplementary material related to this article can be found online at doi:10.1016/j.addma.2021.101921.

4. Conclusion

In summary, we developed a versatile design of printer head for the DIW 3D printing of continuous-fiber reinforced thermoset composites that is applicable to both thermally-curable and UV-curable resins. The extrusion of composite filament is driven by the shear stress imposed on the fiber bundle during the viscous flow of printable inks. The extrusion velocity and fiber volume content can be precisely controlled by adjusting the material and printing parameters, such as ink rheological properties, syringe geometry, and deposition pressure. For the printing of thermally-curable composites, the elastic modulus and ultimate strength in all printing directions are close to those of directly molded samples. This is because during the post-curing of thermally-curable thermoset composites, the interfacial polymerization among the filaments leads to the strong interface connected by covalent bonds. In addition, the slight viscous flow can be leveraged to close the microvoids among filaments and improve the mechanical performance of printed composites. The developed printing method also demonstrates excellent repeatability and reliability in different printing cycles. For the

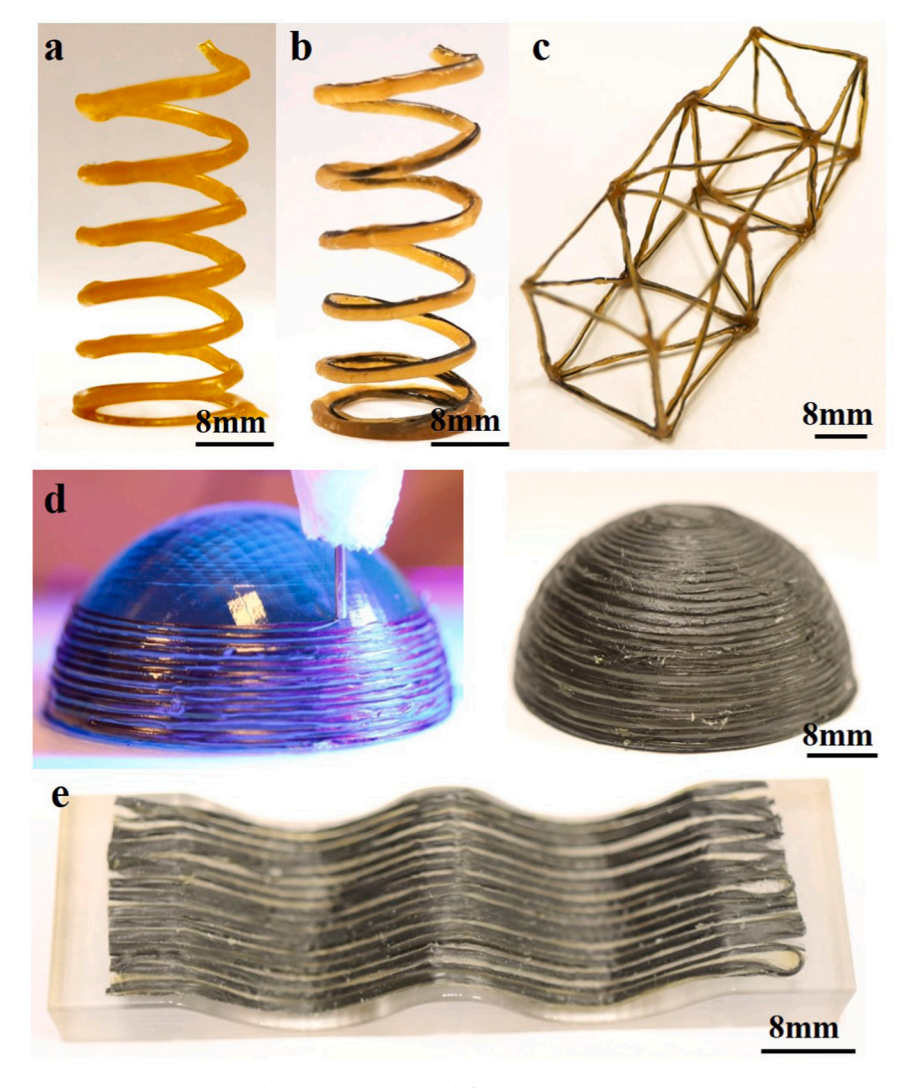


Fig. 8. Appearances of printed springs using UV- curable thermosets (a) with and (b) without carbon fiber. (c) A 3D printed lattice structure. (d) Fiber laying on the spherical surface. (e) Fiber laying on the wavy surface. Scale bars in all these figures are 8 mm.

printing of UV-curable composites, the developed method realized the free-standing 3D printing without Supporting Materials, which enables the efficient deposition of reinforcement fibers in 3D space with or without a substrate. The developed printing method can be readily extended to other thermoset resins (e.g., epoxy) and high-strength reinforcement fibers (e.g., glass fiber). It represents a significant step forward for the advanced manufacturing of polymer composites and potentially disrupts the modern composite design, rapid prototyping, and product development.

CRediT authorship contribution statement

Xu He: Investigation, Visualization, Writing - original draft. Yuchen Ding: Investigation, Visualization. Zepeng Lei: Investigation. Sam Welch: Software. Wei Zhang: Validation, Funding acquisition. Martin Dunn: Validation, Funding acquisition. Kai Yu: Conceptualization, Writing - review & editing, Validation, Funding acquisition.

Declaration of Competing Interest

The authors declare that they have no known competing financial interests or personal relationships that could have appeared to influence the work reported in this paper.

Acknowledgments

K.Y. acknowledges the support from the National Science Foundation (grant number CMMI-1901807). K.Y. and M.D. acknowledge the support of AFOSR grant (FA-20-1-0306; Dr. B.-L. "Les" Lee, Program Manager). W.Z. acknowledges the support from the University of Colorado Boulder and K. C. Wong Education Foundation.

Appendix A. Supporting information

Supplementary data associated with this article can be found in the online version at doi:10.1016/j.addma.2021.101921.

References

- [1] D. Chung, Carbon Composites, Elsevier Inc, New York City, NY, USA, 2016.
- [2] P. Morgan, Carbon Fibers and Their Composites, CRC Press, Taylor & Francis Group, Boca Raton, FL, USA, 2005.
- A.B. Strong, Fundamentals of composites manufacturing: materials, methods and applications, Soc. Manuf. Eng. (2007).
- [4] B. Berman, 3-D printing: the new industrial revolution, Bus. Horiz. 55 (2) (2012) 155–162.
- [5] T.D. Ngo, A. Kashani, G. Imbalzano, K.T.Q. Nguyen, D. Hui, Additive manufacturing (3D printing): a review of materials, methods, applications and challenges, Compos. Part B Eng. 143 (2018) 172–196.
- [6] M. Gebler, A.J.M.S. Uiterkamp, C. Visser, A global sustainability perspective on 3D printing technologies, Energy Policy 74 (2014) 158–167.

- [7] X. Wang, M. Jiang, Z. Zhou, J. Gou, D. Hui, 3D printing of polymer matrix composites: a review and prospective, Compos. Part B Eng. 110 (2017) 442–458.
- [8] P. Parandoush, D. Lin, A review on additive manufacturing of polymer-fiber composites, Compos. Struct. 182 (15) (2017) 36–53.
- [9] B.G. Compton, J.A. Lewis, 3D-printing of lightweight cellular composites, Adv. Mater. 26 (34) (2014) (5930-+).
- [10] Q. Ge, H.J. Qi, M.L. Dunn, Active materials by four-dimension printing, Appl. Phys. Lett. 103 (2013), 131901.
- [11] A.S. Gladman, et al., Biomimetic 4D printing, Nat. Mater. 15 (4) (2016) (413-+).
- [12] B. Bhushan, M. Caspers, An overview of additive manufacturing (3D printing) for microfabrication, Microsyst. Technol. Micro Nanosyst. Inf. Storage Process. Syst. 23 (4) (2017) 1117–1124.
- [13] M. Mao, J. He, X. Li, B. Zhang, Q. Lei, Y. Liu, D. Li, The emerging frontiers and applications of high-resolution 3D printing, Micromachines 8 (4) (2017) 113.
- [14] R. Matsuzaki, M. Ueda, M. Namiki, T.K. Jeong, H. Asahara, K. Horiguchi, T. Nakamura, A. Todoroki, Y. Hirano, Three-dimensional printing of continuousfiber composites by in-nozzle impregnation, Sci. Rep. 6 (2016) 23058.
- [15] J.A. Lewis, Direct ink writing of 3D functional materials, Adv. Funct. Mater. 16 (17) (2006) 2193–2204.
- [16] J.A. Lewis, G.M. Gratson, Direct writing in three dimensions, Mater. Today 7 (7–8) (2004) 32–39.
- [17] G.M. Gratson, M.J. Xu, J.A. Lewis, Microperiodic structures: direct writing of threedimensional webs, Nature 428 (6981) (2004) (p. 386-386).
- [18] C.P. Ambulo, J.J. Burroughs, J.M. Boothby, H. Kim, M.R. Shankar, T.H. Ware, Four-dimensional printing of liquid crystal elastomers, ACS Appl. Mater. Interfaces 9 (42) (2017) 37332–37339.
- [19] A. Kotikian, R.L. Truby, J.W. Boley, T.J. White, J.A. Lewis, 3D printing of liquid crystal elastomeric actuators with spatially programed nematic order, Adv. Mater. 30 (10) (2018) 17061641–17061646.
- [20] J.A. Lewis, Novel inks for direct writing in three dimensions, Digital Fabrication 2005, Final Program and Proceedings, (2005): p. 142-142.
- [21] A. Kotikian, R.L. Truby, J.W. Boley, T.J. White, J.A. Lewis, 3D printing of liquid crystal elastomeric actuators with spatially programed nematic order, Adv. Mater. 30 (2018), 1706164.
- [22] N.G.S. Corporation, Device and method for 3D printing with long fiber reinforcement, US Patent, (2019). US10173410.
- [23] J. Lewicki, et al., Additive manufacturing continuous filament carbon fiber epoxy composites, US Patent, (2017). US20170015060A1.
- [24] K. Tyler, Method and apparatus for continuous composite three-dimensional printing, USA, (2012).
- [25] I.D. Robertson, M. Yourdkhani, P.J. Centellas, J.E. Aw, D.G. Ivanoff, E. Goli, E. M. Lloyd, L.M. Dean, N.R. Sottos, P.H. Geubelle, J.S. Moore, S.R. White, Rapid energy-efficient manufacturing of polymers and composites via frontal polymerization, Nature 557 (7704) (2018) 223–227 (223-+).
- [26] J.S. Moore, et al., 3D printing of thermoset polymers and composites, (2017).
- [27] S. Mazumdar, Opportunities for thermoset resins in the composites industry, (2008).
- [28] R. Zou, Y. Xia, S. Liu, P. Hu, W. Hou, Q. Hu, C. Shan, Isotropic and anisotropic elasticity and yielding of 3D printed material, Compos. Part B Eng. 99 (2016) 506–513.
- [29] S.H. Ahn, M. Montero, D. Odell, S. Roundy, P.K. Wright, Anisotropic material properties of fused deposition modeling ABS, Rapid Prototyp. J. 8 (4) (2002) 248–257.
- [30] Q. Sun, G.M. Rizvi, C.T. Bellehumeur, P. Gu, Effect of processing conditions on the bonding quality of FDM polymer filaments, Rapid Prototyp. J. 14 (2) (2008) 72–80.
- [31] I. Gibson, D. Rosen, B. Stucker. Additive Manufacturing Technologies: 3D Printing, Rapid Prototyping, and Direct Digital Manufacturing, 2nd ed., Springer, 2015 (ISBN 978-1-4939-2113-3).
- [32] M. Namiki, M. Ueda, A. Todoroki, Y. Hirano, R. Matsuzaki, 3D printing of continuous fiber reinforced plastic, Proc. Soc. Adv. Mater. Process. Eng. (2014).
- [33] J. Wang, H. Xie, Z. Weng, T. Senthil, L. Wu, A novel approach to improve mechanical properties of parts fabricated by fused deposition modeling, Mater. Des. 105 (2016) 152–159.
- [34] H.L. Tekinalp, V. Kunc, G.M. Velez-Garcia, C.E. Duty, L.J. Love, A.K. Naskar, C. A. Blue, S. Ozcan, Highly oriented carbon fiber–polymer composites via additive manufacturing, Compos. Sci. Technol. 105 (2014) 144–150.
- [35] F.V.D. Klift, Y. Koga, A. Todoroki, M. Ueda, Y. Hirano, R. Matsuzaki, 3D printing of continuous carbon fibre reinforced thermo-plastic (CFRTP) tensile test specimens, Open J. Compos. Mater. 6 (1) (2015) 18.
- [36] T.H.J. Vaneker, Material extrusion of continuous fiber reinforced plastics using commingled yarn, 1st Cirp Conference on Composite Materials Parts Manufacturing (Cirp Ccmpm 2017), (2017) 66: p. 317–322.
- [37] P. Taynton, K. Yu, R.K. Shoemaker, Y. Jin, H.J. Qi, W. Zhang, Heat- or water-driven malleability in a highly recyclable covalent network polymer, Adv. Mater. 26 (23) (2014) 3938–3942.
- [38] K. Yu, Q. Shi, M.L. Dunn, T. Wang, H.J. Qi, Carbon fiber reinforced thermoset composite with near 100% recyclability, Adv. Funct. Mater. 26 (33) (2016) 6098–6106.

- [39] x Shi, C. Luo, H. Lu, K. Yu, Primary recycling of anhydride-cured engineering epoxy using alcohol solvent, Polym. Eng. Sci. 59 (S2) (2018) E111–E119.
- [40] X. He, Z. Lei, W. Zhang, K. Yu, Recyclable 3D printing of polyimine-based covalent adaptable network polymers, 3D Print. Addit. Manuf. 6 (1) (2019) 31–39.
- [41] X. Shi, D. Soule, Y. Mao, C. Yakacki, H. Lu, K. Yu, A multiscale chemomechanics theory for the solvent – assisted recycling of covalent adaptable network polymers, J. Mech. Phys. Solids 138 (2020), 103918.
- [42] K. Yu, H. Yang, B.H. Dao, Q. Shi, C.M. Yakacki, Dissolution of covalent adaptable network polymers in organic solvent, J. Mech. Phys. Solids 109 (2017) 78–94.
- [43] C.N. Bowman, C.J. Kloxin, Covalent adaptable networks: reversible bond structures incorporated in polymer networks, Angew. Chem. Int. Ed. 51 (18) (2012) 4272–4274
- [44] C.J. Kloxin, T.F. Scott, B.J. Adzima, C.N. Bowman, Covalent adaptable networks (CANS): a unique paradigm in cross-linked polymers, Macromolecules 43 (6) (2010) 2643–2653.
- [45] X. He, D.W. Hanzon, K. Yu, Cyclic welding behavior of covalent adaptable network polymers, J. Polym. Sci. Part B Polym. Phys. 56 (5) (2018) 402–413.
- [46] K. Yu, P. Taynton, W. Zhang, M.L. Dunn, H.J. Qi, Reprocessing and recycling of thermosetting polymers based on bond exchange reactions, RSC Adv. 4 (20) (2014) 10108–10117
- [47] C. Luo, Z. Lei, Y. Mao, X. Shi, W. Zhang, K. Yu, Chemomechanics in the moisture-induced malleability of polyimine-based covalent adaptable networks, Macromolecules 51 (23) (2018) 9825–9838.
- [48] C. Luo, X. Shi, Z. Lei, C. Zhu, W. Zhang, K. Yu, Effects of bond exchange reactions and relaxation of polymer chains on the thermomechanical behaviors of covalent adaptable network polymers, Polymer 153 (2018) 43–51.
- [49] C. Luo, B. Zhang, W. Zhang, C. Yuan, M. Dunn, Q. Ge, K. Yu, Chemomechanics of dual-stage reprocessable thermosets, J. Mech. Phys. Solids 126 (2019) 168–186.
- [50] F.V. Der Klift, Y. Koga, A. Todoroki, M. Ueda, Y. Hirano, R. Matsuzaki, 3D printing of continuous carbon fibre reinforced thermo-plastic (CFRTP) tensile test specimens, Open J. Compos. Mater. 06 (01) (2016) 18–27.
- [51] K.-i Mori, T. Maeno, Y. Nakagawa, Dieless forming of carbon fibre reinforced plastic parts using 3D printer, Procedia Eng. 81 (2014) 1595–1600.
- [52] N. Li, Y. Li, S. Liu, Rapid prototyping of continuous carbon fiber reinforced polylactic acid composites by 3D printing, J. Mater. Process. Technol. 238 (2016) 218–225.
- [53] C. Yang, X. Tian, T. Liu, Y. Cao, D. Li, 3D printing for continuous fiber reinforced thermoplastic composites: mechanism and performance, Rapid Prototyp. J. 23 (2017) 209–215.
- [54] X. Tian, T. Liu, C. Yang, Q. Wang, D. Li, Interface and performance of 3D printed continuous carbon fiber reinforced PLA composites, Compos. Part A Appl. Sci. Manuf. 88 (2016) 198–205.
- [55] X. Tian, T. Liu, Q. Wang, A. Dilmurat, D. Li, G. Ziegmann, Recycling and remanufacturing of 3D printed continuous carbon fiber reinforced PLA composites, J. Clean. Prod. 142 (2017) 1609–1618.
- [56] G.D. Goh, V. Dikshit, A.P. Nagalingam, G.L. Goh, S. Agarwala, S.L. Sing, J. Wei, W. Y. Yeong, Characterization of mechanical properties and fracture mode of additively manufactured carbon fiber and glass fiber reinforced thermoplastics, Mater. Des. 137 (2018) 79–89.
- [57] D. Jiang, D. Smith, Mechanical behavior of carbon fiber composites produced with fused filament fabrication, in Solid Freeform Fabrication Symposium Proceedings, (2016).
- [58] L.J. Love, V. Kunc, O. Rios, C.E. Duty, A.M. Elliott, B.K. Post, R.J. Smith, C.A. Blue, The importance of carbon fiber to polymer additive manufacturing, J. Mater. Res. 29 (17) (2014) 1893–1898.
- [59] H.L. Tekinalp, V. Kunc, G.M. Velez-Garcia, C.E. Duty, L.J. Love, A.K. Naskar, C. A. Blue, S. Ozcan, Highly oriented carbon fiber–polymer composites via additive manufacturing, Compos. Sci. Technol. 105 (2014) 144–150.
- [60] G. Liao, Z. Li, Y. Cheng, D. Xu, D. Zhu, S. Jiang, J. Guo, X. Chen, G. Xu, Y. Zhu, Properties of oriented carbon fiber/polyamide 12 composite parts fabricated by fused deposition modeling, Mater. Des. 139 (2018) 283–292.
- [61] W. Zhang, C. Cotton, J. Sun, D. Heider, B. Gu, B. Sun, T.W. Chou, Interfacial bonding strength of short carbon fiber/acrylonitrile-butadiene-styrene composites fabricated by fused deposition modeling, Compos. Part B Eng. 137 (2018) 51–59.
- [62] N. Nawafleh, E. Celik, Additive manufacturing of short fiber reinforced thermoset composites with unprecedented mechanical performance, Addit. Manuf. 33 (2020), 101109.
- [63] M. Invernizzi, G. Natale, M. Levi, S. Turri, G. Griffini, UV-assisted 3D printing of glass and carbon fiber-reinforced dual-cure polymer composites, Materials 9 (7) (2016) 583.
- [64] B.G. Compton, J.A. Lewis, 3D-printing of lightweight cellular composites. Adv. Mater. 26 (34) (2014) 5930–5935.
- [65] P. Taynton, H. Ni, C. Zhu, K. Yu, S. Loob, Y. Jin, H.J. Qi, W. Zhang, Repairable woven carbon fiber composites with full recyclability enabled by malleable polyimine networks, Adv. Mater. 28 (15) (2016) 2904–2909.